Vehicle Performance Assessment Using the OBD2 Port and Artificial Neural Network

Mauricio Sobrino y Arjona-Guzman and Moises Jimenez-Martinez*, *Member, IAENG, and Sergio G. Torres-Cedillo*

Abstract—There is a growing body of literature that recognises the importance of vehicle performance assessment to evaluate and improve vehicle dynamics and fuel consumption. This study set out to investigate the usefulness of the artificial neural networks (ANNs) to predict the vehicle performance curves and acceleration responses. The experimental measurements are obtained from an OBD2 port of a Suzuki SX4 sedan, and the torque-power engine curves are achieved according to the SAE standard SAEJ1491 JUL2006. Therefore, it is demonstrated that the vehicle performance can be improved and predicted using vehicle measurements, gear ratios, and dynamic rolling radius. Then, the actual paper reports that ANNs can be employed as a non-parametric model to predict vehicle behaviour, improve comfort, and reduce the steps between gear changes.

Index Terms—Torque-power engine curve; OBD2; vehicle dynamics; ANN.

Fig. 1: Schematic of the torque-power curve.

I. INTRODUCTION

THE acceleration capability depends on longitudinal vehicle dynamics, which is the result of body car characteristics (body stiffness). The powertrain performance is not only determined by the ideal behavioural capability itself but also includes losses. The more torque an engine produces and transmits, the more force it can exert at the rim of a flywheel of a given radius to move the vehicle.

On an engine, the torque increases as the rotational speed increases from idle to a certain value of RPM where the torque reaches its maximum, after which it falls as the rotational speed continues to increase above this point. Meanwhile, the power increases with rotational speed up to and past the point of maximum torque. However, at higher rotational speeds, the engine starts to be limited by the amount of air that it can take, and the torque then decreases more rapidly than the rotational speed increase; therefore, the power also decreases, as shown in Fig. 1.

Performance analysis can be used to improve stability with assistance. In many vehicles, it can be used to improve vehicle performance and reduce fuel consumption or improve towing loads. The amount of torque or power an engine can generate determines if the vehicle would be capable of carrying a certain amount of mass or encountering a slope, as well as the maximum speed the vehicle can achieve. The maximum acceleration in a given gear is obtained when

the maximum torque is obtained, so the best efficiency is obtained at the maximum torque.

To measure and obtain the torque-power curves, a dynamometer is used. Another option is to use the OBD2 port and the diagnosis computer of the vehicle. On Board Diagnostics II (OBD2) is a diagnostic system that regulates vehicle emissions. It also checks the status of all sensors involved in emissions [1] and is also used for failure simulations while the vehicle is under normal conditions during its operation, instead of at static test benches with off-board diagnosis [2].

Environmental regulations have evolved to strict levels, and there is a change in the means of propulsion, such as hybrid or electric vehicles. Although green vehicles are being mass-produced, due to their cost, it is not possible to replace conventional vehicles in emerging countries; due to this, it is essential to improve and evaluate the impact of emissions from vehicles that use fossil fuels. Toxicity indices are tested in static (stationary) or dynamic (transient) conditions; for the latter, a PEMS (portable emissions measurement system) can be used, and the adjustment and correction of the torque improve the toxicity assessment under operating conditions [3]. Different proposals have been made to integrate OBD to improve vehicle performance or monitor it. Sentoff et al.[4] analysed the inertia loads to meet the air quality emissions requirements. Bishop et al. [5] built engine maps using data gathered from OBD and portable emissions measurement systems. Fayazi et al. [6] used the OBD to evaluate the environmental impact and included the road profile [7]. Jiang et al. [8] proposed a maintenance system on a diesel heavy-duty vehicle using OBD. Mayyas et al. [9] proposed a model to predict the powertrain temperature profiles by OBD based on the battery current and voltage relationship to the vehicle speed [10]. Duarte et al. [11] evaluated the effect of battery state of charge (SOC) on fuel consumption.

Xie et al. [12] proposed an integrated system based on long

M. Sobrino y Arjona-Guzman is a postgraduate student in automotive engineering, Tecnologico de Monterrey, Toluca, México (e-mail:a01169223@tec.mx). M. Jimenez-Martinez is a Professor at the School of Engineering and Science, Tecnologico de Monterrey, Puebla, México (corresponding author, e-mail: moisesjimenezmartinez@gmail.com).

S.G. Torres-Cedillo is a Professor at the School of Engineering, Universidad Nacional Autónoma de México, Centro Tecnológico FES Aragón, Edo.Méx., México. (e-mail:sgtorres.c@gmail.com).
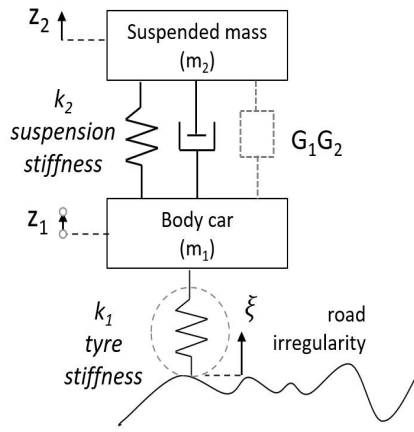
Fig. 2: Simplified active quarter suspension.

short-term memory (PA-LSTM) for building an emission prediction model using PEMS and OBD, and the responses can be transmitted by Bluetooth [13]. Turkson et al. [14] proposed an artificial neural network using OBD signals for engine calibration. Martinelli et al. [15] integrated a machine learning system with the signals of an electronic control unit to prevent theft attacks. Vasavi et al. [16] integrated an artificial neural network with OBD signals for predictive maintenance. On board measurements and neural networks can be used to evaluate the powertrain performance [17]. Orlowska et al. [18] presented neural estimators of the mechanical state variables of the electrical drive system. The nonmeasurable state variables are estimated using multilayer feedforward neural networks. Malik et al. [19] analysed driver behaviours using OBD and artificial intelligence to analyse body motion and gestures (hand, feet and head movements). Agostino et al. [20] analysed the driver intention on a vehicle with a manual gearbox, using an OBD port as an alternative way for electrification of rear wheels in front-driven vehicles.

In this work, an ANN is proposed to evaluate the vehicle performance and acceleration responses based on OBD measurements. Vehicle responses using an on-board measurement system can be used to predict behaviour as a power-torque curve and accelerations.

II. DISCOMFORT EVALUATION.

To evaluate suspension responses as discomfort, road holding and body-wheel working space, the responses from acceleration and the road are compared using the power spectral density of the road irregularity $\left(1/\omega^2\right)$ or $\left(1/\left(\omega^2 + \omega_c^2\right)\right)$ depending on the excitation levels.

The quarter system model of a passively suspended road vehicle is shown in Fig. 2, and the equations of motion are defined by:

$$m_1 \ddot{z}_1 - r_2\left(\dot{z}_2 - \dot{z}_1\right) - k_2\left(z_2 - z_1\right) + k_1\left(z_1 - \xi\right) = 0 \quad (1)$$

$$m_2 \ddot{z}_2 + r_2\left(\dot{z}_2 - \dot{z}_1\right) + k_2\left(z_2 - z_1\right) = 0 \quad (2)$$

The discomfort is evaluated by computing the standard deviation of the vertical vehicle body acceleration (σ_{Fz2}).

The standard deviation of the tire radial force (σ_{Fz1}) is related to road holding. The variation in the tire radial force can lead to a loss of contact with the ground and poor handling ability, influencing the active safety due to lateral forces influencing the stability and passive safety [21], [22]. The standard deviation of the relative displacement between the wheel and vehicle body $(\sigma_{Fz2} - \sigma_{Fz1})$, known as the working space, is related to design and packaging constraints, as well as to wheel lateral vibrations. The transfer functions between the displacement ξ and z_1 and ξ and z_2 are expressed by

$$Z_1\left(j\omega\right) = \frac{k_1\left(k_2 + jr_2\omega - m_2\omega^2\right)}{k_1k_2 + jk_1r_2\omega - \left(k_2m_1 + k_1m_2 + k_2m_2\right)\omega^2 ... \atop -jr_2\left(m_1 + m_2\right)\omega^3 + m_1m_2\omega^4}$$

(3)

$$Z_2\left(j\omega\right) = \frac{k_1\left(k_2 + jr_2\omega\right)}{k_1k_2 + jk_1r_2\omega - \left(k_2m_1 + k_1m_2 + k_2m_2\right)\omega^2 ... \atop -jr_2\left(m_1 + m_2\right)\omega^3 + m_1m_2\omega^4}$$

(4)

The transfer functions between road irregularity ξ and body acceleration $\ddot{Z}_2\left(H_1\right)$, ξ and road holding $\sigma_{Fz1}\left(H_2\right)$, and ξ and relative displacement $\left(\sigma_{Fz2} - \sigma_{Fz1}\right)\left(H_3\right)$ are shown in Equations (5-7), respectively.

$$H_1\left(j\omega\right) = -\omega^2 Z_2\left(j\omega\right) \quad (5)$$

$$H_2\left(j\omega\right) = k_1\left(1 - Z_1\left(j\omega\right)\right) \quad (6)$$

$$H_3\left(j\omega\right) = Z_2\left(j\omega\right) - Z_1\left(j\omega\right) \quad (7)$$

The displacement ξ (road irregularity) may be represented by a random variable defined by a stationary and ergodic stochastic process. The power spectral density (PSD) is expressed by

$$PSD_{\xi 2}\left(\omega\right) = \frac{A_v\omega_c}{\omega_c^2 + \omega^2} \quad (8)$$

where $\omega_c = av$ and a (rad/m) depend on the shape of the road irregularity spectrum. For a stable system, the PSD takes the form

$$PSD_l\left(\omega\right) = \left|H_l\left(j\omega\right)\right|^2 PSD_{\xi q}\left(\omega\right) \quad (9)$$

For $l = 1$, PSD_l represents the PSD of the vertical acceleration of the vehicle body; $l = 2$ PSD_l represents the PSD of the vertical force applied between the tire and road; and for $l = 3$, PSD_l represents the PSD of the relative displacement between the wheel and vehicle body. The index $q = 1, 2$ refers to the $1S - PSD$ and $2S - PSD$, respectively. The discomfort is expressed by:

$$\sigma_{\ddot{Z}2}^2 = \frac{1}{2}A_b v\left[\frac{1}{m_2^2}\left(\frac{\left(m_2 + m_1\right)k_2^3}{r_2}\right) + k_1r_2\right] \quad (10)$$

For an active system using gains G_1 and G_2 and the shape of road irregularity, $a(rad/m)$ discomfort can be evaluated for 1 and 2 degrees of freedom, respectively.

$$\sigma^2_{\ddot{Z}2} = A_b \upsilon \frac{1}{2} \frac{G_1^2}{G_2 m_2} \tag{11}$$

$$\sigma^2_{\ddot{Z}2} = A_\upsilon a \upsilon \frac{1}{2} \frac{G_1^2 \left(G_1 + a\upsilon G_2\right)}{G_2 m_2 \left(G_1 + a\upsilon \left(G_2 + a\upsilon m_2\right)\right)} \tag{12}$$

III. TIME HISTORY PREDICTION.

The time history can be evaluated using its trend by

$$\bar{Z}_t - \phi_i \bar{Z}_{t-1} - \phi_2 \bar{Z}_{t-2} - ... - \phi_p \bar{Z}_{t-p} =$$
$$a_t - \theta_1 a_{t-1} - ... - \theta_q a_{q-1} \tag{13}$$

where $\bar{Z}_t$ is the regression of its own past values, and its expected value $E(Y)$ is described by

$$E\left[Y\right] = E\left[f\left(\theta, X\right) + \varepsilon\right] = E\left[f\left(\theta, X\right)\right] =$$
$$f\left(\theta, EX\right) = f\left(\theta, X\right) \tag{14}$$

If function $f\left(\cdot\right)$ and the autoregressive parameters θ are known, Y can be estimated with X. If function $f\left(\cdot\right)$ can be realized by a neural network, the time series can be predicted by

$$Y = X_{M+1} = h\left[\sum_{n=1}^{N} w_{nI}^2 f\left(\sum_{m=1}^{M} w'_{mI} x_m + b_I^1\right) + b_j^2\right]$$
$$\tag{15}$$

Another method to forecast the mechanical behaviour is by support vector machine [12], as expressed by:

$$f\left(x\right) = w \cdot \phi\left(x\right) + b = \sum_{i=1}^{K} \left(\alpha_1 - \alpha_1^*\right) K\left(x, x_i\right) + b \tag{16}$$

By its nature, an artificial neural network has been implemented to analyse nonlinear phenomena; it considers all the connections between inputs and responses to evaluate the effect of interconnections (synapses). Synaptic weights are internal parameters that are modified based on the process successive responses; they extract the relationships of inputs and expected behaviour among input, hidden and output layers [23]. The extraction of information is the learning process, and the acquired knowledge is organized to cluster the patterns found, which can be used to predict future values. The fundamental element is the neuron that transmits impulses; it has three main parts: the cell body, dendrites and axon. The cell body is responsible for processing the information that is transferred from dendrites. The function of dendrites is to connect and recollect information from other neurons or external elements. Axons are used to guide between neurons, and their terminations are known as synaptic terminals. The main components of the ANN are input signals $(x_1, x_2, x_3, \ldots . x_n)$, synaptic weights $(w_1, w_2, w_3 \ldots, w_n)$, an activation threshold also known as bias (θ) that functions as a trigger towards the output, the activation potential (u), the activation function (g) and the output signal (y). Figure 3 shows a feed forward network.
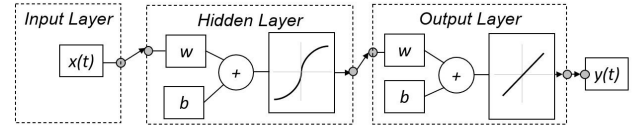
Fig. 3: ANN topology.

The activation function influences the training process; it is selected as a sigmoid function because it combines different behaviours and is expressed by

$$g\left(u\right) = \frac{1}{1 + e^{\beta \cdot u}} \tag{17}$$

To prevent noise in the input data, Bayesian regularization $F = E_D$ is used, including an additional term taking into account the sum of square errors E_w as follows:

$$F = \beta E_D + \alpha E_w \tag{18}$$

Where E_w is defined by

$$E_w = \sum_{i=1}^{N} w_i^2 \tag{19}$$

Depending on the objective function parameter (β, α) relationship, overfitting can occur if $\beta >> \alpha$; in other cases, the training focuses on weight reduction tolerating higher errors if $\alpha >> \beta$ [24].

The topology of the network has 40 hidden neurons; 70% of the samples are used for training, and 15% are used for validation and testing. The parameters used to train and validate the networks are the vehicle parameters and computed as RPM, power, torque, velocity and acceleration.

IV. EXPERIMENTAL PERFORMANCE EVALUATION

To obtain the signals of torque-power curves, the USB connection is used by using the ELM327 scanner and OBD2 port, which is located in the driver's footwell, in the centre console or even under the passenger seat. To perform the analysis, the gear ratios and the dynamic rolling radius are obtained. The dynamic rolling radius r_e, also known as the effective rolling radius, gives the relationship of rolling speed or angular velocity of the wheel ω_w and forward velocity v, as expressed by

$$r_e = \frac{v}{\omega_w} \tag{20}$$

The effective rolling radius changes with the amount of tire deflection, which has a value between the unloaded R and loaded radius [25]. It is obtained by measuring the angular velocity of the wheel and the forward vehicle speed. Table I provides the experimental data obtained from an experimental test to measure this variable.

The gear ratio, also known as the speed ratio, is the ratio of the angular velocity of the input gear to the angular velocity of the output gear. The final gear ratio considers the effect of the gearbox (N_t) and the differential (N_f) by

TABLE I: Effective rolling radius at different speeds.

Test speed	20 km/hr	30 km/hr	40km/hr
1	0.3065	0.3359	0.3135
2	0.3035	0.3138	0.3147
3	0.3006	0.3116	0.3128
Average	0.3035	0.3127	0.3137

TABLE II: Effective rolling radius at different speeds.

Shift	RPM	Speed (m/s)	N_{tf}	N_t	Deviation
1st	2606.5	5.567	15.542	3.670	2.45%
2nd	2140.3	8.555	8.303	1.960	2.05%
3rd	2250.2	12.651	5.904	1.342	2.44%
R	2354.0	5.442	14.360	3.391	3.00%

$$N_{tf} = N_t N_f \qquad (21)$$

where N_{tf} is the final gear ratio. However, the final gear ratio is also the speed ratio, as expressed by

$$N_{tf} = \frac{\omega_e}{\omega_w} \qquad (22)$$

where ω_e is the rotational speed of the engine. OBD2 can only give data of the engine rotational speed and vehicle velocity (v). Eq. 23 presents a relationship that relates the linear velocity with rotational velocity:

$$v = \omega_w r \qquad (23)$$

Using 22 and 23, the final gear ratio in terms of engine angular velocity and vehicle speed is rewritten as follows

$$N_{tf} = \frac{\omega_e}{v} r \qquad (24)$$

where the differential gear ratio N_{tf}=4.235.

With a velocity of 45.5 km/hr, the engine rotates at 2140.3 RPM. Using (2) and (5), the gear ratios are found, as shown in Table II.

At high shifts, the gear ratio decreases because the vehicle needs less torque. Meanwhile, at low shifts, including reversal, a high gear ratio is needed to increase the torque applied to the wheels, and the vehicle is capable of overcoming inertia.

$OBD2$ is unable to give us directly the torque or the power delivered by the engine in real time. The only kinematic parameter of the engine that we can read by means of the $OBD2$ port is the angular velocity. Analysing the vehicle dynamics fundamental equation, the following is obtained:

$$a = \left(\frac{N_{tf} n_{tf} T_t}{r_e} - R_h - R_x - D_A - W\sin\phi \right) * \frac{1}{mM_f} \qquad (25)$$

where a is the longitudinal acceleration, T_e is the torque delivered by the engine, η_{tf} is the total transmission efficiency, R_h is the towing force, and R_x is the rolling resistance force. D_A is the aerodynamic drag force, W is the weight of the vehicle, ϕ is the road slope angle, m is the mass of the vehicle, and M_f is the mass factor.

The test is performed over a horizontal surface (zero road slope angle). In addition, the vehicle is not towing anything; thus, the R_h and $W\sin\phi$ terms are equal to zero. The rolling resistance force is expressed for low and high speed respectively by

$$f_r = 0.01 \left(1 + \frac{v}{100} \right) \qquad (26)$$

$$f_r = f_o + 3.24 f_s \left(1 + \frac{v}{100} \right)^{2.5} \qquad (27)$$

where v is the forward vehicle velocity in MPH and f_r, f_o are tire inflation pressure constants

However, the aerodynamic drag force is

$$D_A = \frac{1}{2} \rho C_A v^2 \qquad (28)$$

where ρ is the air density, C_a is the drag coefficient and A is the front area of the vehicle. The vehicle under study is shown in Fig. 4, with a drag coefficient of 0.32 and a mass of 1650 kg.
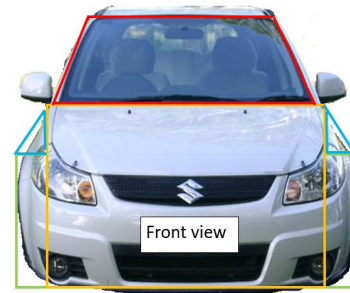
Fig. 4: Method used to calculate the vehicle frontal area.

The mass factor index depends on the operating shift and differential gear ratio (N_{tf}) as follows:

$$M_f = 1 + 0.04 N_{tf} + 0.0025 N_{tf}^2 \qquad (29)$$

The rolling resistance and drag forces depend on the forward velocity (v), so we can express v in terms of the engine angular speed by solving for v in Equation 24. The longitudinal acceleration (a) in terms of ω_e shows that the angular acceleration is equal to the derivative of the rotational speed with respect to time. Then, based on the relationship between longitudinal and rotational acceleration:

$$a = \alpha_w r_e \qquad (30)$$

The angular acceleration of the engine α_e is related to the rotational acceleration of the wheel α_w as follows:

$$0.8\alpha_w = \frac{\alpha_e}{N_{tf}} r_e \qquad (31)$$

The longitudinal acceleration can be rewritten as:

$$a = \frac{d\omega_e}{dt} \frac{r_e}{N_{tf}} \qquad (32)$$

An equation for the torque in terms of the rotational engine speed is expressed by

$$T_e = \frac{\left(\left(\left(\frac{d\omega_e}{dt}\frac{r}{N_{tf}}\right)(mM_f) + 0.01\left(W + \frac{W\frac{\omega_e}{N_{tf}}r}{100}\right) + \vartheta\right)\right)^2}{\frac{N_{tf}\eta_{tf}}{r}}$$

(33)

where $\vartheta = \frac{1}{2}\rho C_A \left(\frac{\omega_e}{N_{tf}}r\right)^2$.

The test was performed from idle speed to 6000 RPM in the first shift, obtaining the engine rotational speed versus time from OBD2. The final gear ratio N_{tf} for the first shift was calculated as well as the effective rolling radius r_e and the aerodynamic drag force parameters.

V. RESULTS AND DISCUSSION

What is striking about the vehicle behaviour monitoring in this study case is that the responses are nonlinear and generated from diverse sources. The main one is the non-linear components such as the wheels, but other origins might be the road irregularities, bad driving habits, number of passengers, payload, fuel level. Another cause would be the environmental conditions such as temperature could change the wheel forces. Therefore, it is certainly important to consider these different causes to implement them in an on-board system (OBD). Therefore, the OBD can be improved by using ANNs which are non-parametric model obtained from empirical data.

Figure 5 presents the results from the 1st shift to the 5th shift (Figs. 5a-5e), while the shift increases the expected accelerations. The ideal behaviour is compared with the losses by the powertrain system. The second evaluation includes the transmission and rolling resistance (trans + rolling), finally including the transmission, rolling resistance and drag coefficient using the ANN.

To evaluate the constant engine power, it is approached with the tractive effort that the vehicle can reach maximum power. To predict the losses of the driveline, the losses by the components and the drag coefficient, the changes between gears indicate the biases of the transmission system, as shown in Figure 5. In the first gear (Fig. 5a), the behaviour with losses is less than ideal but has a similar tendency due to the effect of the drive train, as well as when including the rolling and drag coefficients. In the second speed, it is observed that the effects of rolling and the drag coefficient are similar to each other but have a greater effect than only when considering the effects of the drive train. From the third gear, the difference between accelerations is greater due to the inertial effects of the components, the change in traction forces at the points of contact of the wheels, and the drag coefficient, which increases its effect at a higher speed, as can be seen from Figure 5b.

The acceleration curve is an on-time measurement of a vehicle torque requirement to minimize the steps between gears due to shift inertial phases. Figure 6 compares the steps between the gears, although this behaviour is expected to be reduced to improve the comfort during acceleration and to improve the longitudinal vehicle dynamics. To evaluate the vehicle with the powertrain, the rolling resistance and drag coefficient are isolated and compared with the ANN result to analyse its prediction.

The experimental torque-power curves (Fig. 7) are below the ideal curves. This loss of performance can be explained

(a)

(b)

(c)

(d)

(e)
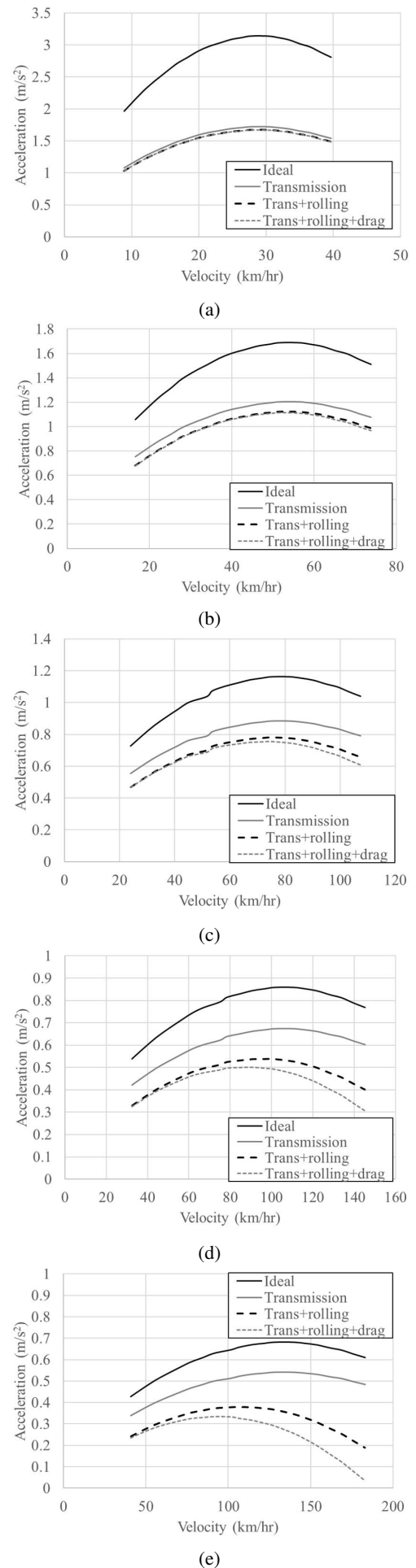
Fig. 5: Acceleration in (a) 1st gear, (b) 2nd gear, (c)3rd gear, (d)4th gear and (e) 5th gear.
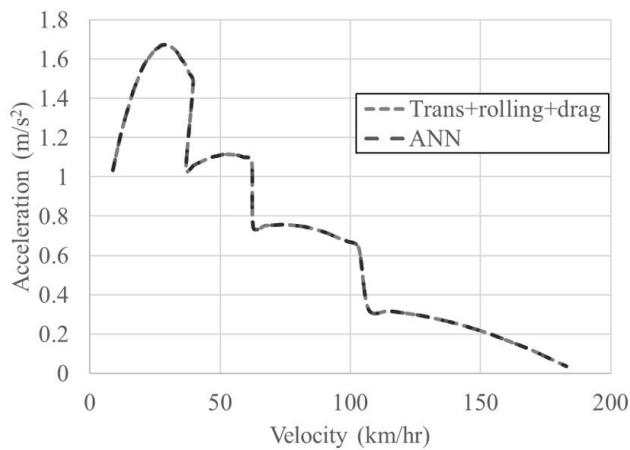
Fig. 6: Acceleration prediction using the ANN.
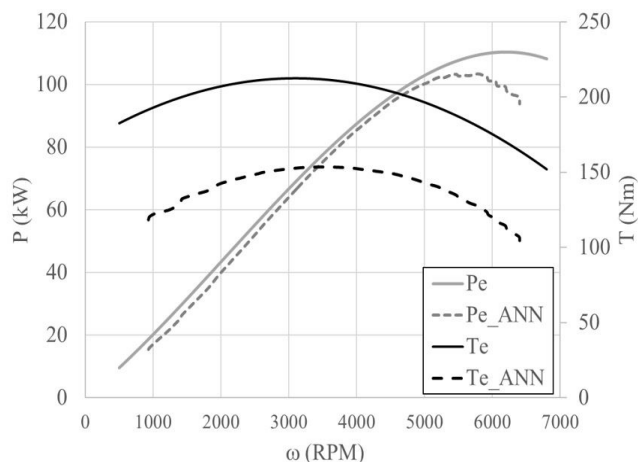
Fig. 7: Torque-power curve prediction using the ANN.

by the altitude of Mexico City. An increase in altitude causes the atmospheric pressure to decrease, and the percentage of oxygen present per unit volume of air decreases as well. A vehicle operating at a rotational speed below its maximum torque point is in an unstable speed regime. If it slows down by a small amount, the torque decreases, and its speed will fall further. Conversely, if the speed increases, then the torque increases and the speed increases even more, so the driver must compensate for these variations by closing or opening the throttle. The maximum errors found in the prediction are 0.13% for the acceleration and 0.02% for the power and torque.

The development of systems to evaluate vehicle performance can be used in internal combustion vehicles to reduce polluting emissions, while for hybrid or electric vehicles, systems can be implemented to reduce energy consumption by improving efficiency and performance. On the other hand, the analysis can be used to improve traction forces.

VI. CONCLUSION

The purpose of the current study was to analyse the responses of a vehicle in transitory systems rather than static ones. Consequently, it was considered different kind of variables such as passenger numbers, environmental conditions, and vehicle maintenance. It was also included the driving habits which can suddenly change the vehicle response.

The engine torque is usually measured under steady state conditions on a dynamometer. Then, the predicted and measured torques are reduced employing the rotational inertia components condensed as the system losses. The evaluation necessarily needs to be obtained from real conditions. It can therefore be noted that the OBD responses using together with ANNs can be identified the engine characteristic curves without a dynamometer. Since there are methods to simulate air conditions, there are others static and dynamic variables that must be evaluated under operating conditions. It is well known that engine torque will tend to increase and resist slowing. Therefore, if it speeds up by a small amount, the torque will decrease to prevent an increase in speed.

It was also noted that user's comfort can be improved by reducing steps between the gear acceleration responses. This reduction has a direct effect over the longitudinal dynamic and the tractive forces. Another observation might be that the combination between this response, the overall powertrain efficiency, and losses can be employed to reduce fuel consumption. Therefore, the present work reports that it is necessarily considering the vehicle feedback, leading to a higher torque to acquire a better overall efficiency.

Finally, it was stated that the OBD needs to incorporate acceleration to improve the dynamic vehicle behaviour under distinct conditions such as roll, dive and squat. There is also a significant finding, this kind of active systems to improve vehicle performance on longitudinal dynamic and stability for lateral dynamics.

REFERENCES

[1] D. Rimpas, A. Papadakis, and M. Samarakou, "Obd-ii sensor diagnostics for monitoring vehicle operation and consumption," *Energy Reports*, vol. 6, pp. 55–63, 2020, technologies and Materials for Renewable Energy, Environment and Sustainability.

[2] F. Richert and D. Brückner, "Automated validation process for on-board-diagnosis functions," *IFAC Proceedings Volumes*, vol. 43, no. 7, pp. 727–732, 2010, 6th IFAC Symposium on Advances in Automotive Control.

[3] Łukasz Rymaniak, P. Lijewski, M. Kamińska, P. Fuć, B. Kurc, M. Siedlecki, T. Kalociński, and A. Jagielski, "The role of real power output from farm tractor engines in determining their environmental performance in actual operating conditions," *Computers and Electronics in Agriculture*, vol. 173, p. 105405, 2020.

[4] K. M. Sentoff, L. Aultman-Hall, and B. A. Holmén, "Implications of driving style and road grade for accurate vehicle activity data and emissions estimates," *Transportation Research Part D: Transport and Environment*, vol. 35, pp. 175–188, 2015.

[5] J. D. Bishop, M. E. Stettler, N. Molden, and A. M. Boies, "Engine maps of fuel use and emissions from transient driving cycles," *Applied Energy*, vol. 183, pp. 202–217, 2016.

[6] S. A. Fayazi, A. Vahidi, and A. Luckow, "A vehicle-in-the-loop (vil) verification of an all-autonomous intersection control scheme," *Transportation Research Part C: Emerging Technologies*, vol. 107, pp. 193–210, 2019.

[7] L. Yang, S. Zhang, Y. Wu, Q. Chen, T. Niu, X. Huang, S. Zhang, L. Zhang, Y. Zhou, and J. Hao, "Evaluating real-world co2 and nox emissions for public transit buses using a remote wireless on-board diagnostic (obd) approach," *Environmental Pollution*, vol. 218, pp. 453–462, 2016.

[8] Y. Jiang, J. Yang, Y. Tan, S. Yoon, H.-L. Chang, J. Collins, H. Maldonado, M. Carlock, N. Clark, D. McKain, D. Cocker, G. Karavalakis, K. C. Johnson, and T. D. Durbin, "Evaluation of emissions benefits of obd-based repairs for potential application in a heavy-duty vehicle inspection and maintenance program," *Atmospheric Environment*, vol. 247, p. 118186, 2021.

[9] A. R. Mayyas, M. Omar, P. Pisu, A. Al-Ahmer, A. Mayyas, C. Montes, and S. Dongri, "Comprehensive thermal modeling of a power-split hybrid powertrain using battery cell model," *Journal of Power Sources*, vol. 196, no. 15, pp. 6588–6594, 2011.

[10] B. Sun, T. Gu, P. Wang, T. Zhang, and S. Wei, "Optimization design of powertrain parameters for electromechanical flywheel hybrid electric vehicle." *IAENG International Journal of Applied Mathematics*, vol. 52, no. 2, pp. 450–457, 2022.

[11] G. Duarte, R. Varella, G. Gonçalves, and T. Farias, "Effect of battery state of charge on fuel use and pollutant emissions of a full hybrid electric light duty vehicle," *Journal of Power Sources*, vol. 246, pp. 377–386, 2014.

[12] H. Xie, Y. Zhang, Y. He, K. You, B. Fan, D. Yu, B. Lei, and W. Zhang, "Parallel attention-based lstm for building a prediction model of vehicle emissions using pems and obd," *Measurement*, vol. 185, p. 110074, 2021.

[13] S. hyun Baek and J.-W. Jang, "Implementation of integrated obd-ii connector with external network," *Information Systems*, vol. 50, pp. 69–75, 2015.

[14] R. F. Turkson, F. Yan, M. K. A. Ali, and J. Hu, "Artificial neural network applications in the calibration of spark-ignition engines: An overview," *Engineering Science and Technology, an International Journal*, vol. 19, no. 3, pp. 1346–1359, 2016.

[15] F. Martinelli, F. Mercaldo, A. Orlando, V. Nardone, A. Santone, and A. K. Sangaiah, "Human behavior characterization for driving style recognition in vehicle system," *Computers Electrical Engineering*, vol. 83, p. 102504, 2020.

[16] S. Vasavi, K. Aswarth, T. Sai Durga Pavan, and A. Anu Gokhale, "Predictive analytics as a service for vehicle health monitoring using edge computing and ak-nn algorithm," *Materials Today: Proceedings*, vol. 46, pp. 8645–8654, 2021, 3rd International Conference on Materials, Manufacturing and Modelling.

[17] C. Guardiola, C. Vigild, F. De Smet, and K. Schusteritz, "From obd to connected diagnostics: a game changer at fleet, vehicle and component level**ford-upv collaboration on connected diagnostics is funded by eu h2020 ict-56-2020 grant 957258 assist-iot. c guardiola also acknowledges spanish agencia estatal de investigación grant pid2019-108031rb-c21." *IFAC-PapersOnLine*, vol. 54, no. 10, pp. 558–563, 2021, 6th IFAC Conference on Engine Powertrain Control, Simulation and Modeling E-COSM 2021.

[18] T. Orlowska-Kowalska and M. Kaminski, "Application of the obd method for optimization of neural state variable estimators of the two-mass drive system," *Neurocomputing*, vol. 72, no. 13, pp. 3034–3045, 2009, hybrid Learning Machines (HAIS 2007) / Recent Developments in Natural Computation (ICNC 2007).

[19] M. Malik and R. Nandal, "A framework on driving behavior and pattern using on-board diagnostics (obd-ii) tool," *Materials Today: Proceedings*, 2021.

[20] M. D'Agostino, M. Naddeo, and G. Rizzo, "Development and validation of a model to detect active gear via obd data for a through-the-road hybrid electric vehicle," *IFAC Proceedings Volumes*, vol. 47, no. 3, pp. 6618–6623, 2014, 19th IFAC World Congress.

[21] S. M. Mostafa, S. A. Salem, and S. M. Habashy, "Predictive model for accident severity." *IAENG International Journal of Computer Science*, vol. 49, no. 1, pp. 110–124, 2022.

[22] M. Jimenez-Martinez, "Artificial neural networks for passive safety assessment." *Engineering Letters*, vol. 30, no. 1, pp. 289–297, 2022.

[23] Şahin Yildirim and İbrahim Uzmay, "Neural network applications to vehicle's vibration analysis," *Mechanism and Machine Theory*, vol. 38, no. 1, pp. 27–41, 2003.

[24] M. Jimenez-Martinez and M. Alfaro-Ponce, "Effects of synthetic data applied to artificial neural networks for fatigue life prediction in nodular cast iron," *Journal of the Brazilian Society of Mechanical Sciences and Engineering*, vol. 43, p. 9, 2021.

[25] H. B. Pacejka, *Tyre and Vehicle Dynamics*, United Kingdom: Butterworth-Heinemann, 2006.

M. Jimenez-Martinez was born in México in 1979. He received his PhD in Mechanical Engineering from IPN in 2015. He became a Member (M) of IAENG in 2020. His current research interests include Artificial Neural Network in Mechanical design. Finite Element Analysis and Nonlinear Analysis.

Dr. Jimenez is member of the Canadian Society of Mechanical Engineering(CSME) and is member of the Mexican National System Research (SNI).

S.G. Torres Cedillo is a PhD in Mechanical Engineering with extensive experience in mechanical vibrations and rotodynamic. His PhD degree was obtained at The University of Manchester, UK in 2015. Since then, he has continued exploring non-invasive inverse methods for the unbalance identification applied to rotodynamic systems using techniques such as artificial neural networks, inverse problem method.

Currently, he is a Professor SNI level 1 at Centro Tecnológico at FES Aragon UNAM.

M. Sobrino y Arjona Guzmán was born in Mexico in 1992. He is a postgraduate student in Automotive Engineering and received a bachelorś degree in Mechanical and Electrical Engineering in 2016, both at the Tecnológico de Monterrey in Mexico City. His current research interests include vehicle dynamics and vehicle structural analysis using finite element method with either linear or non-linear approaches.

He joined Stellantis (former Fiat Chrysler Automobiles), Mexico City in 2015, where currently is a Senior Vehicle Packaging Engineer performing virtual design validations to instill packaging feasibility within the primary zone of a vehicle architecture.